

Stereodynamics of Metal–Ligand Assembly: What Lies Beneath the “Simple” Spectral Signatures of C_2 -Symmetric Chiral Chelates

Jiyoung Jung,^[a, b] Junyong Jo,^[a] Moitree Laskar,^[a] and Dongwhan Lee*^[a]

Abstract: A series of C_2 -symmetric chiral tetra-dentate ligands were prepared by using [4,5]- or [5,6]-pinene-fused 2,2'-bipyridyl units that are supported across a rigid arylene–ethynylene backbone. These conformationally pre-organised chelates support stable 1:1 metal complexes, which were fully characterised by UV/Vis, fluorescence, circular dichroism (CD), and $^1\text{H NMR}$ spectroscopy. A careful inspection of the exciton-coupled circular dichroism (ECCD) and $^1\text{H NMR}$ spectra of the reaction mixture in solution, however, revealed the evolution and decay of in-

intermediate species en route to the final 1:1 metal–ligand adduct. Consistent with this model, mass spectrometric analysis revealed the presence of multiple metal complexes in solution at high ligand-to-metal ratios, which were essentially unobservable by UV/Vis or fluorescence spectroscopic techniques. Comparative studies with a bi-dentate model system have fully established

the functional role of the π -conjugated ligand skeleton that dramatically enhances the thermodynamic stability of the 1:1 complex. In addition to serving as a useful spectroscopic handle to understand the otherwise “invisible” solution dynamics of this metal–ligand assembly process, temperature-dependent changes in the proton resonances associated with the chiral ligands allowed us to determine the activation barrier (ΔG^\ddagger) for the chirality switching between the thermodynamically stable but kinetically labile (*P*)- and (*M*)-stereoisomers.

Keywords: C_2 symmetry • circular dichroism • ligands • self-assembly • switching

Introduction

Helical arrangements of self-folded objects are frequently encountered in biological systems, with prominent examples including DNA and protein secondary structures. Transition-metal complexes and clusters having topologically related axial chirality have been prepared and studied extensively to develop and refine intuitive models of stereoinduction (that is, chirality transfer from the ligand to the metal)^[1] that have been widely applied and tested across various disciplines including: 1) supramolecular self-assembly,^[2] 2) asymmetric catalysis,^[3,4] and 3) recognition of small-molecule inhibitors and probes by enzymes^[5] and nucleic acids.^[6]

In the assembly of such chiral complexes, binding to the metal centre enhances intramolecular contacts between chiral ligand fragments that are brought into close proximity, thereby “amplifying” the effects of asymmetric steric bias. As a consequence, only a finite number of stereoisomers emerge from multiple chiral components that converge at a single metal centre. For helicates that are comprised of two or more intertwined coaxial ligand chains running along the long axis to support multiple metal centres, the configurational stability of the metal-centred chirality is enhanced further.^[7] In addition to the energetic preference induced by close van der Waals contacts and other non-covalent interactions, molecular symmetry plays a critical role in these complexes by significantly reducing the number of potentially competing structural isomers and simplifying the reaction coordinates.

Within this context, multi-dentate ligands having C_2 point-group symmetry have been studied extensively as building blocks for the assembly of chiral metal complexes and clusters. As shown in Figure 1, restricted rotation around the C–C bond connecting two *ortho*-substituted aromatic ring systems results in two mirror-image isomers. Prominent examples of such chiral biaryl systems include BINOL^[8] and BINAP (Figure 1),^[9] which continue to inspire the design, synthesis, and applications of a large family of structural analogues.^[10] In addition to functioning as chiral bi-dentate ligands to support various oxophilic catalytic sites, the parent BINOL system can also serve as a chiral hydrogen-bond donor. An increasing number of Brønsted acids, such as **A–E** (Figure 1), have also been built upon the axially chiral binaphthyl platform to catalyse a wide range of asymmetric organic transformations involving carbon–carbon or carbon–heteroatom bond formation.^[11]

In the binaphthyl-based C_2 -symmetric systems shown in Figure 1, the conformational stability (and therefore practi-

[a] Dr. J. Jung, J. Jo, M. Laskar, Prof. Dr. D. Lee
Department of Chemistry, Indiana University
800 East Kirkwood Avenue, Bloomington, Indiana 47405 (USA)
Fax: (+)812-855-8300
E-mail: dongwhan@indiana.edu

[b] Dr. J. Jung
Current Address: Department of Chemistry
Slippery Rock University, 1 Morrow Way
Slippery Rock, Pennsylvania 16057 (USA)

Supporting information for this article is available on the WWW under <http://dx.doi.org/10.1002/chem.201204216>; it contains experimental details and supporting data.

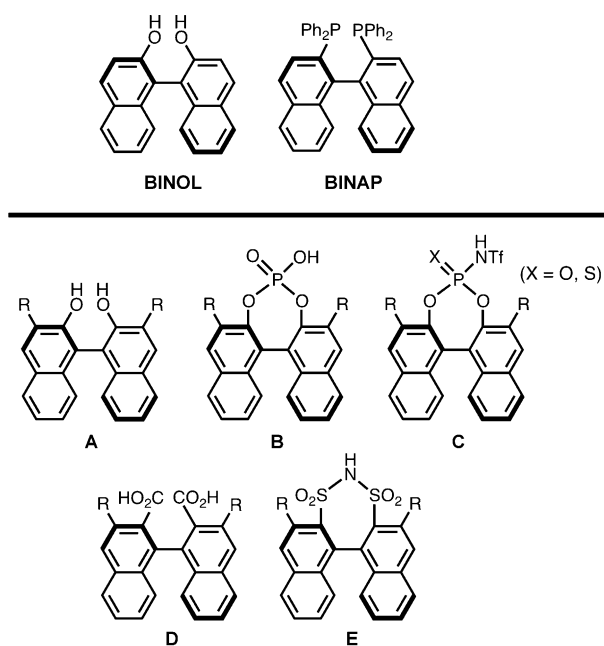


Figure 1. Chemical structures of axially chiral ligands BINOL and BINAP, and structurally related C_2 -symmetric chiral Brønsted acids **A–E** derived from the conformationally well-defined binaphthyl platform. For each molecule, only the (*R*)-enantiomer is shown.

cal utility) of the two atropisomers derives from the direct aryl–aryl linkage and the presence of bulky *ortho* substituents, which collectively result in a prohibitively high energy barrier for their structural interconversion through C–C bond rotation under ambient conditions. In contrast, the C_2 -symmetric systems **F–I** shown in Figure 2^[12–14] have ethynylene-based spacer units between the two *ortho*-substituted aryl fragments to allow for relatively unrestricted rotation around the “axle” that is perpendicular to the C_2 axis.

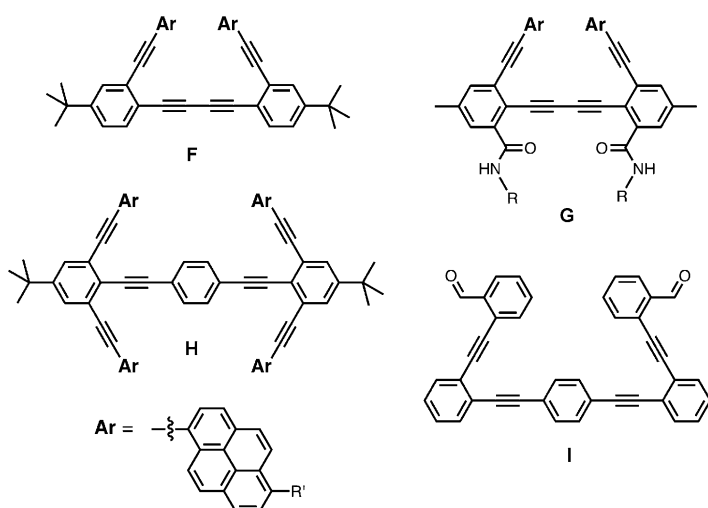
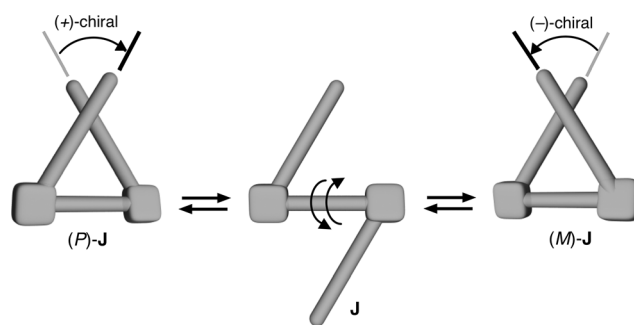


Figure 2. Chemical structures of C_2 -symmetric arylene–ethynylene systems **F–I** as “ π -extended” analogues of the biaryl systems shown in Figure 1.



Scheme 1. Dynamic interconversion between the right-handed (*P*)-**J** and left-handed (*M*)-**J** conformation of a C_2 -symmetric structure **J**. With achiral “arm” units rotating around the horizontal “axle”, (*P*)-**J** and (*M*)-**J** are mirror images of each other, and therefore isoenergetic. Installation of chiral auxiliaries in the arm units should establish a diastereomeric relationship between (*P*)-**J** and (*M*)-**J**, the energy difference between which drives asymmetric folding toward one helical screw sense, either *P* or *M*, over the other.

The low energy barrier of the bond rotation around the arylene–ethynylene unit,^[15] such as those in **F–I**, offers additional advantages for the operation of these molecular “hinges”, “tweezers”, and other conceptually related molecular switches and devices.^[16] As shown in Scheme 1, the system can readily sample either right-handed, (*P*)-**J**, or left-handed, (*M*)-**J**, helical conformation through the “unfolded” intermediate **J**.

Research elsewhere has demonstrated that the conformational switching shown in Scheme 1 can be driven by: 1) π – π stacking interactions (for **F** and **H**),^[12] 2) hydrogen-bonding interactions (for **G**),^[13] or 3) reversible formation of covalent bonds with exogenously added amines (for **I**).^[14] Notably, condensation reactions between the dialdehyde **I** and chiral diamines afford macrocyclic Schiff bases, in which a well-defined spatial relationship between the two arylene–ethynylene-based local chromophores gives rise to strong exciton-coupled circular dichroism (ECCD) signals.^[17–24]

We have recently shown that a topologically related C_2 -symmetric arylene–ethynylene platform can support two 2,2'-bipyridyl (bipy) ligands that converge at a single metal centre to define a *cis*-divacant octahedral coordination environment.^[25,26] Depending on the absolute spatial relationship between the two π -extended bipy units with respect to the bis(ethynylphenyl) linker, both the right-handed (*P*)- and left-handed (*M*)-isomers were obtained for the structurally characterised [Zn(**L1**)(OTf)₂] complex (Figure 3). The restricted swivelling motion of the hinged bipy units that “flap” around the rigid “axle” of **L1** is reminiscent of a Dutch door (Scheme 2).

As shown in Figure 3, the octahedral complex [Zn(**L1**)(OTf)₂] has two *cis* coordination sites that are occupied by the triflate ligands, which can potentially exchange with exogenously added substrates. Without any inherent asymmetric bias, however, the mirror-image (*P*)- and (*M*)-isomers are isoenergetic, which precludes potential applications of **L1** and its metal complexes for chiral recognition or asymmetric chemical transformation.

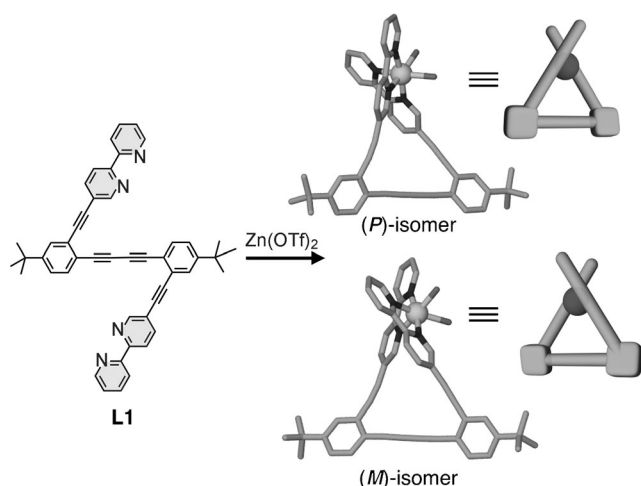
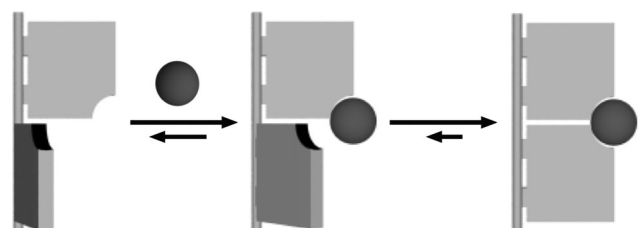


Figure 3. Chemical structure of **L1** and capped-stick representations of the solid-state structure of its metal complex $[\text{Zn}(\text{L1})(\text{OTf})_2]$ constructed from the X-ray coordinates.^[25] For the two terminally bound triflate ligands, only the oxygen donor atoms are shown for clarity.



Scheme 2. A cartoon-type representation of the Dutch-door-like swiveling motions of **L1** having two bipy ligand units as “movable panels” to bind the metal ion (shown as a dark sphere) to form a discrete 1:1 complex.

As a logical first step to preferentially stabilise one helical sense over the other (Scheme 1), we thus decided to prepare chiral derivatives **L2^R**, **L2^S**, **L3^S** and **L4^R** (Figure 4) of the parent system **L1** (Figure 3). With these newly synthesised C_2 -symmetric ligands, we investigated their metallation to form chiral complexes. A combination of UV/Vis, fluorescence, circular dichroism (CD), and ^1H NMR spectroscopic studies have allowed for a detailed understanding of: 1) the reaction pathways leading to metal–ligand assembly, and 2) the thermodynamic stability and kinetic lability of the resulting chiral metal complexes. Specifically, we have confirmed experimentally that a simple 1:1 binding model (Scheme 2), suggested by previous Job plot analysis on **L1**, is an oversimplification of the actual equilibrium in solution.^[25] The reaction coordinates actually involve multiple oligomeric species co-existing at low metal-to-ligand ratios, which converge to a discrete and stable 1:1 adduct with an increased loading of metal ions. In addition, low-temperature ^1H NMR studies revealed the presence of both (*P*)- and (*M*)-isomers in solution, which interconvert through a low energy barrier (ΔG^\ddagger). A coherent mechanistic picture thus emerges for the stereodynamics of this metal–ligand system,

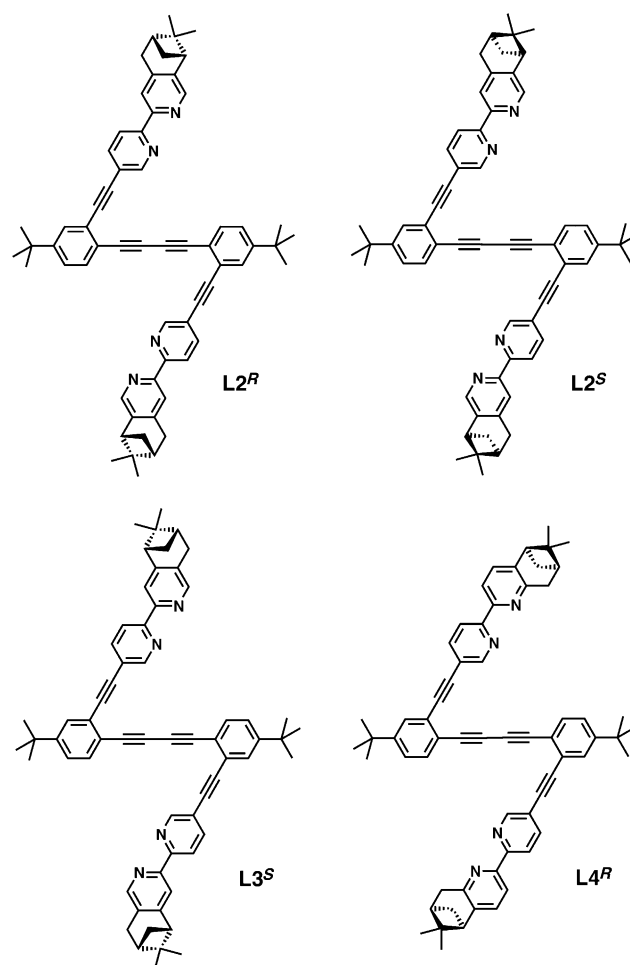
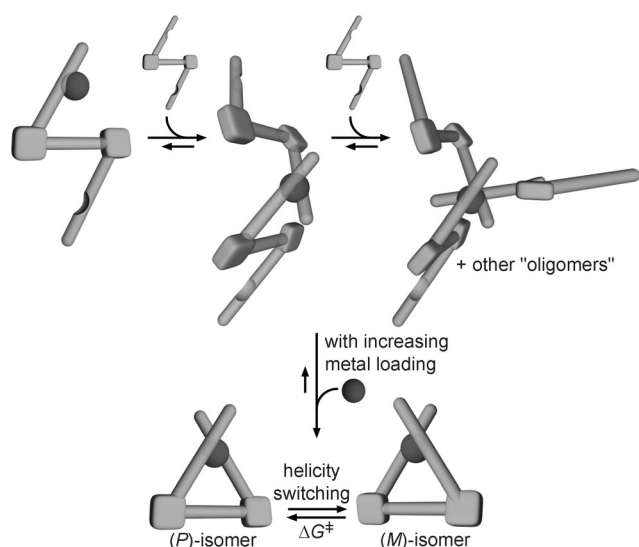


Figure 4. Chemical structures of the chiral N_4 ligands.

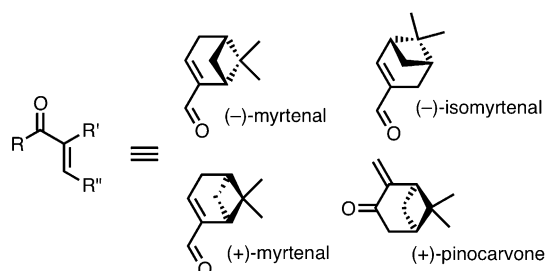
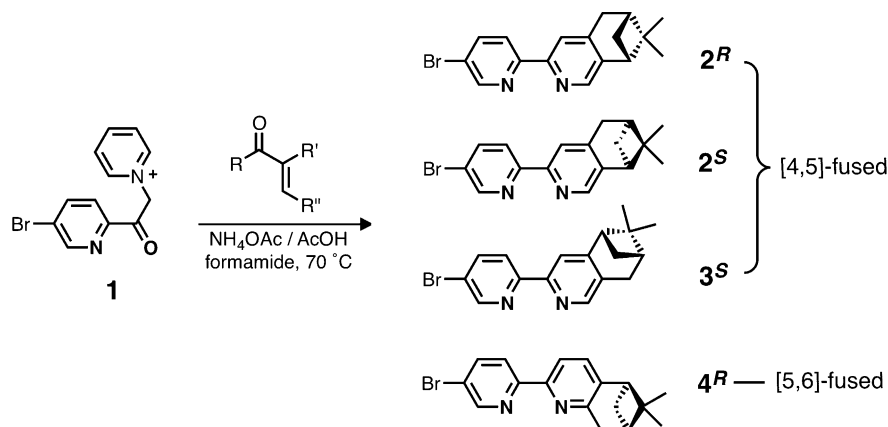
which is summarised in Scheme 3 and detailed in the following sections.

Background: Ligand design for helical folding: The solid-state structures of the achiral complex $[\text{Zn}(\text{L1})(\text{OTf})_2]$ (Figure 3) served as a good starting point for our design of chiral tetra-dentate ligands to support an asymmetric coordination environment. As shown in Figure 3, the pseudo- C_2 -symmetric arrangement of **L1** around the metal centre brings the two bipy groups into close proximity. We thus reasoned that annulation of either the [4,5]- or [5,6]-position of the bipy ligand with appropriate chiral auxiliaries would introduce sufficient steric bias to energetically differentiate the (*P*)- and (*M*)-isomers of the resulting metal complex (Scheme 3). For this objective, we have chosen derivatives of CHIRAGEN ligands (Scheme 4) pioneered by von Zelewsky and others.^[14,27–31]

By using chiral pinene precursors,^[27] these [4,5]- or [5,6]-annulated bipy derivatives^[28] can readily be prepared in enantiomerically pure forms.^[14,29–31] The absolute configuration of the stereogenic centres residing in the pinene portion of the CHIRAGEN compound translates directly to the ab-



Scheme 3. Concentration-dependent dynamics of the metal complexes supported by the chiral Dutch-door-type ligand in solution.



Scheme 4. Synthesis of bromo-substituted chiral bipyridines.

solute configuration of the their metal complexes, which have been studied extensively in supramolecular chemistry and asymmetric catalysis.^[1d,29–31] We thus anticipated that structural modification of the parent system **L1** with pinene-annulated bipy units **2–4** (Scheme 4) should allow us to control the absolute stereochemistry of helical folding upon metallation.

Results and Discussion

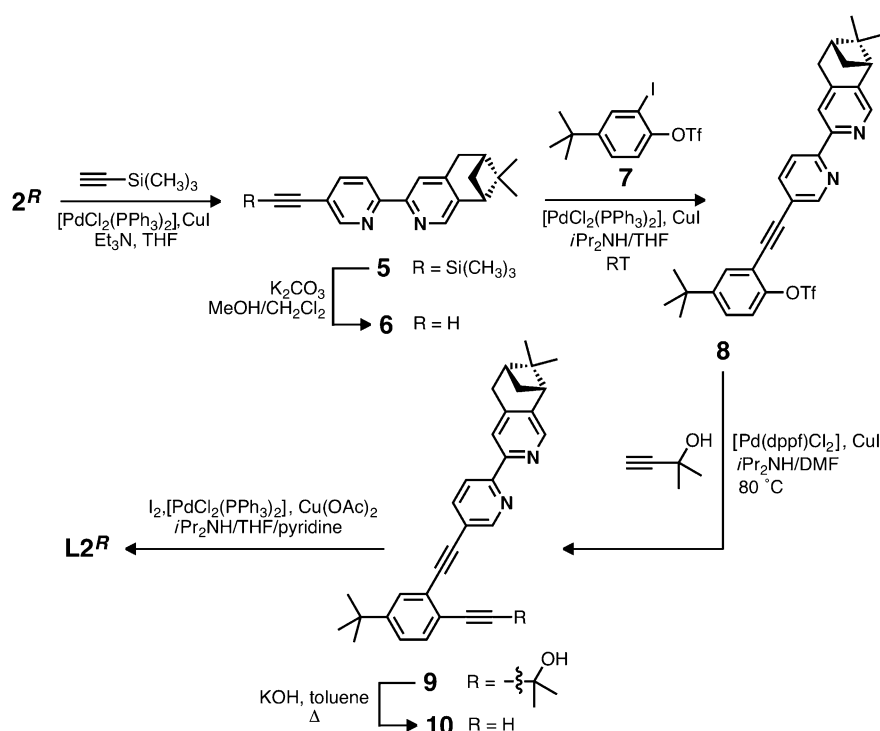
Ligand synthesis: A highly modular synthetic route that we have developed for the synthesis of **L1**^[25] was readily adapted to prepare **L2^R**, **L2^S**, **L3^S** and **L4^R** (Figure 4) in a straightforward manner. The key building blocks shown in Scheme 4 were prepared through a common Kröhnke pyridinium intermediate **1**,^[32] which was subjected to condensation reactions with either (–)- or (+)-myrtenal^[33] in the presence of ammonium acetate to furnish pineno-[4,5]-fused bipy **2^R** and **2^S**, respectively, as an enantiomeric pair.^[34] Another [4,5]-fused bipy derivative **3^S** was prepared from (–)-isomyrtenal by using the same synthetic protocol.^[35,36] To investigate the effects of annulation closer to the nitrogen donor atom on the asymmetric steric bias upon metallation, the pineno-[5,6]-fused bipy **4^R** was synthesised by using (+)-pinocarvone, which was prepared by oxidation of (–)- α -pinene.^[37]

As outlined in Scheme 5, consecutive Sonogashira–Hagihara cross-coupling reactions transformed **2^R** into **10**, which was subjected to oxidative homo-coupling conditions to afford **L2^R**. By taking similar synthetic routes, compounds **L2^S**, **L3^S** and **L4^R** were prepared and fully characterised (Schemes S1–S3 in the Supporting Information). As anticipated, the optical rotations of **L2^R** ($[\alpha]_D^{23} = -64^\circ$ ($c = 0.980$, CHCl_3)) and **L2^S** ($[\alpha]_D^{23} = +64^\circ$ ($c = 0.985$, CHCl_3)) at $T = 23^\circ\text{C}$ were of the same magnitude but opposite in sign, which fully establishes their enantiomeric stereochemical relationship.

¹H NMR spectroscopy of metal-

ligation reactions: With the series of chiral ligands **L2^R**, **L2^S**, **L3^S** and **L4^R** newly prepared, we first investigated their metallation in solution by ¹H NMR spectroscopy. Upon treatment with $\text{Zn}(\text{OTf})_2$ (2 equiv) at $T = 298\text{ K}$, the ¹H NMR spectrum of **L2^R** in CDCl_3 displayed significant shifts in the proton resonances associated with the bipy portion of the molecule

(Figure 5). Under these conditions, the resonances from the bis(ethynylphenyl) “axle” part of the molecule remained largely unchanged. The ¹H NMR spectral pattern of the reaction mixture is essentially identical to that of the independently prepared and characterised (see below) mononuclear zinc(II) complex $[\text{Zn}(\text{L2}^{\text{R}})(\text{OTf})_2]$, thus confirming the formation of a discrete 1:1 complex. Similar observations



Scheme 5. Synthetic route to $L2^R$.

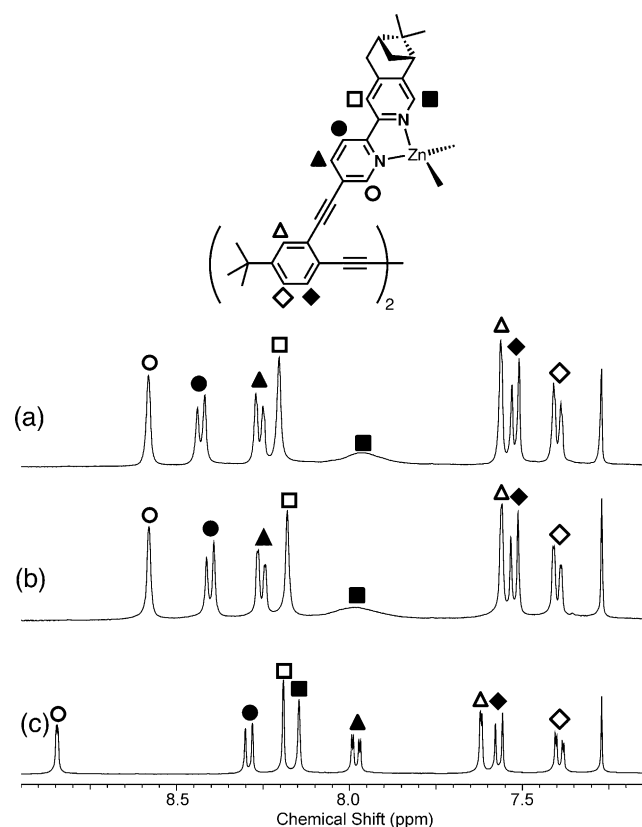


Figure 5. Partial ^1H NMR spectra of a) the isolated $[\text{Zn}(\text{L}2^R)(\text{OTf})_2]$ complex, b) $\text{L}2^R$ treated with two equivalents of $\text{Zn}(\text{OTf})_2$ and c) the free ligand $\text{L}2^R$ in CDCl_3 at $T = 298\text{ K}$.

were made for $\text{L}3^S$ (Figure S1 in the Supporting Information).

In contrast to the well-resolved spectral changes observed for the metallation of $\text{L}2^R$ and $\text{L}3^S$ built with pineno-[4,5]-fused bipy motifs, structurally related $\text{L}4^R$ having pineno-[5,6]-fused bipy units showed broad and complicated ^1H NMR resonances upon treatment with zinc(II) (Figure S2 in the Supporting Information). Such a convoluted spectral pattern implies the evolution of multiple species in solution with different metal-to-ligand stoichiometry (Scheme 3; see below). With annulation at the [5,6]-positions imposing significant steric constraints upon metallation of the bipy units, the formation of discrete 1:1 metal complexes might be unfavourable for $\text{L}4^R$.

Metallation-induced helical folding: To obtain structural evidence for the metallation-induced structural folding of $\text{L}2^R$, its zinc(II) complex was prepared on a preparatory scale. An equimolar mixture of the free ligand and $\text{Zn}(\text{OTf})_2$ in a CH_2Cl_2 -MeCN mixed solvent system furnished the anticipated 1:1 adduct, which was isolated and fully characterised (see the Supporting Information). As shown in Figure 5, the ^1H NMR spectra of the free ligand $\text{L}2^R$ and the corresponding zinc(II) complex $[\text{Zn}(\text{L}2^R)(\text{OTf})_2]$ are well-resolved. Although the simple spectral patterns are consistent with the molecular C_2 symmetry of the ligand, which is retained both for the free ligand and in the metal complex, the resonances from the H3' ($\Delta\delta = 0.18\text{ ppm}$), H4' ($\Delta\delta = 0.31\text{ ppm}$) and H3 ($\Delta\delta = 0.10\text{ ppm}$) protons showed downfield shifts due to the de-shielding effects of the nearby metal centre (see Figure 6 for the proton numbering scheme). On the other hand, the resonances corresponding to the protons H6 and H6' of the bipy unit, which are at the *ortho*-positions to the nitrogen donor atoms, undergo upfield shifts ($\Delta\delta = 0.25\text{ ppm}$ for H6; $\delta = 0.10\text{ ppm}$ for H6') as a result of the compensating shielding effects from the neighbouring bipy π system.^[38] Such spectral shifts confirmed that, upon metallation, the bipy units of $\text{L}2^R$ undergo a conformational change from *transoid* to *cisoid*.^[39,40]

Additional structural information for metallated $\text{L}2^R$ was obtained by two-dimensional (2D) ROESY ^1H NMR spectroscopy on the isolated $[\text{Zn}(\text{L}2^R)(\text{OTf})_2]$ complex (Figure 6 and Figure S3 in the Supporting Information). Although conformational analysis by using NOE was rather challenging for $[\text{Zn}(\text{L}2^R)(\text{OTf})_2]$, which showed rather weak NOE correlations between its remotely located pinene moieties

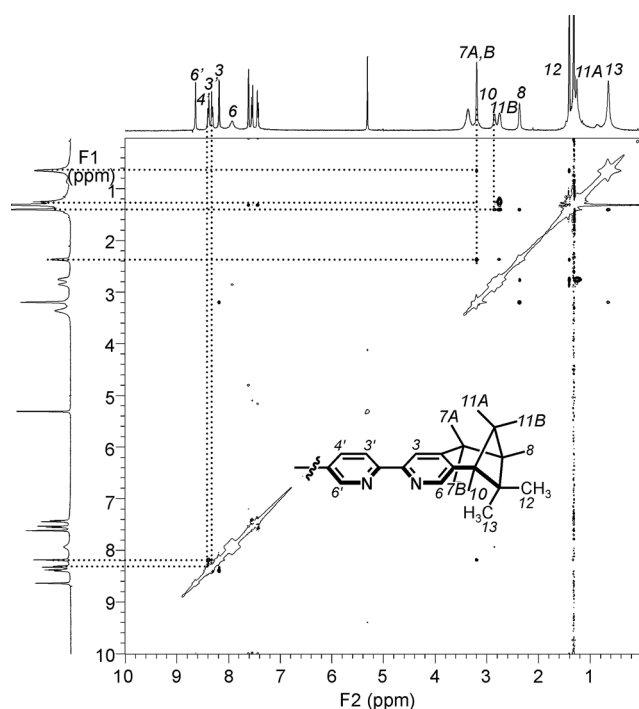


Figure 6. The 2D ROESY spectrum of $[\text{Zn}(\text{L}2^R)(\text{OTf})_2]$ in CD_2Cl_2 at $T=298\text{ K}$, and the numbering scheme of the ligand used for the assignment of the resonances. Due to broadening, H7A and H7B appear as a singlet.

and suffered from significant broadening of the diastereotopic H7 protons, several cross-peaks that were observed provided compelling evidence for the helical spatial arrangement of the ligand (Figure 6).

Compared with the ROESY spectrum of the free ligand $\text{L}2^R$ (Figure S4 in the Supporting Information), the prominent H3–H3' and H3–H4' cross-peaks of the metallation product (Figure 6 and Figure S3 in the Supporting Information) confirm twisting of the bipy fragment from a *transoid* to a *cisoid* conformation upon metal binding. As for the pinene portion of the molecule, the metal-free $\text{L}2^R$ showed only an H7–H8 cross-peak, whereas the corresponding zinc(II) complex, $[\text{Zn}(\text{L}2^R)(\text{OTf})_2]$, displayed additional NOE correlation peaks for H7–H11A and H7–H13. Most importantly, the H10–H12 cross-peak of $[\text{Zn}(\text{L}2^R)(\text{OTf})_2]$ establishes a close spatial relationship between the two pinene moieties, which can only be established by coordination to the metal ion as shown in Figure 3.

UV/Vis and fluorescence spectroscopic signatures of metal-

lation: The ^1H NMR spectroscopic studies described in the previous section have provided compelling experimental evidence that the pinene-fused chiral ligand $\text{L}2^R$ can bind zinc(II) to form a discrete 1:1 complex, in a manner similar to the behaviour of its achiral and less bulky analogue $\text{L}1$.^[25] We thus decided to investigate metal binding in solution by UV/Vis (Figure 7a) and fluorescence (Figure 7b) spectroscopic titration.

As shown in Figure 7a, metallation of $\text{L}2^R$ resulted in a gradual decrease in the absorption at $\lambda_{\text{max}}=315\text{ nm}$ with

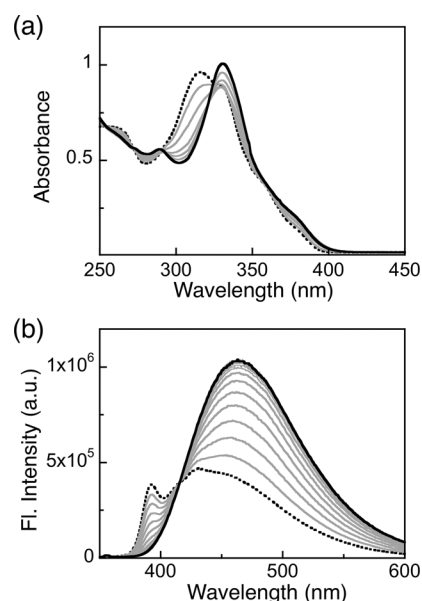


Figure 7. a) UV/Vis and b) fluorescence ($\lambda_{\text{exc}}=320\text{ nm}$) spectra of $\text{L}2^R$ (a) $10\ \mu\text{M}$; b) $1.0\ \mu\text{M}$) in MeCN titrated with $\text{Zn}(\text{OTf})_2$ (a) 0–2.5; b) 0–2 equiv) at $T=298\text{ K}$.

concomitant development of a longer-wavelength transition at $\lambda_{\text{max}}=330\text{ nm}$. A similar ratiometric change was also observed in the fluorescence spectra (Figure 7b), with a large enhancement in the emission at $\lambda_{\text{max}}=465\text{ nm}$ (from the metal complex) and a correlated decrease in the emission at $\lambda_{\text{max}}=390\text{ nm}$ (from the free ligand) across an isoemissive point at $\lambda=415\text{ nm}$. A Job plot analysis (Figure S5 in the Supporting Information) established a 1:1 binding stoichiometry, which is consistent with the results from ^1H NMR spectroscopy shown in Figures 5 and 6. Similar results were obtained for the titration of $\text{L}3^S$ with zinc(II) (Figure S6 in the Supporting Information).

Taken together, the presence of the chiral directing groups in the pineno-[4,5]-fused ligands $\text{L}2^R$ or $\text{L}3^S$ does not detrimentally affect the inherent metal-binding ability and the characteristic optical response of the π -conjugated bis-(bipy) unit of the “unsubstituted” parent ligand system $\text{L}1$.^[25] In contrast, the ligand $\text{L}4^R$, having the pinene motif fused at the [5,6]-position of the bipy unit, produced a complicated Job plot (Figure S7 in the Supporting Information). Apparently, the presence of the rigid ring-fused substituents pointing towards the primary coordination sphere prevents the formation of discrete metal complexes of well-defined stoichiometry. This postulation was also supported by the complicated ^1H NMR spectral patterns observed for the reaction mixture of $\text{L}4^R$ and $\text{Zn}(\text{OTf})_2$ (Figure S2 in the Supporting Information).

CD spectroscopic studies of chirality transfer: As a metal complex with a closed-shell d^{10} system, the UV/Vis spectrum of $[\text{Zn}(\text{L}2^R)(\text{OTf})_2]$ is dominated by the π - π^* electronic transitions, which are only slightly shifted from those of the free ligand $\text{L}2^R$ and are therefore not very informative (Fig-

ure 7a and Figure S8 in the Supporting Information). In contrast, the CD spectrum of $[\text{Zn}(\text{L2}^R)(\text{OTf})_2]$ displays sharply defined bisignate features, which is distinctly different from that of the free ligand L2^R (Figure 8).

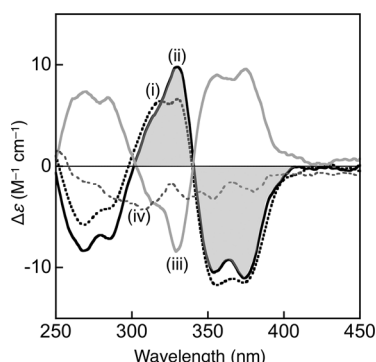


Figure 8. CD spectra of i) isolated $[\text{Zn}(\text{L2}^R)(\text{OTf})_2]$ (black dotted line), ii) L2^R treated with $\text{Zn}(\text{OTf})_2$ (1.5 equiv; black solid line), and iii) L2^S treated with $\text{Zn}(\text{OTf})_2$ (1.5 equiv; grey solid line), compared with that of iv) free ligand L2^R (grey dashed line) in MeCN at $T = 298$ K.

As shown in Figure 8, the CD spectrum of $[\text{Zn}(\text{L2}^R)(\text{OTf})_2]$, either: 1) isolated and re-dissolved in solution (black dotted line), or 2) generated in situ by mixing the metal salt and the ligand in solution (black solid line), displays a negative couplet (shaded in grey) across $\lambda = 340$ nm. The enantiomeric metal complex $[\text{Zn}(\text{L2}^S)(\text{OTf})_2]$, generated in situ by treating the ligand L2^S with $\text{Zn}(\text{OTf})_2$, shows an essentially superimposable UV/Vis spectrum to that of $[\text{Zn}(\text{L2}^R)(\text{OTf})_2]$, but produces a mirror-image ECCD spectrum with a positive couplet (Figure 8; grey solid line). A direct correlation is thus established between the *R* versus *S* point chirality residing at the pinene-fused bipy portion of the ligand and the ECCD signal observed upon metal binding. This empirical relationship is generally applicable for other transition-metal ions including iron(II), copper(II), cobalt(II), nickel(II), cadmium(II) and mercury(II) (Figure S9 in the Supporting Information), whereas their fluorescence-response profile showed significant metal-dependent variations (Figure S10 in the Supporting Information).

Convoluting reaction pathways of metal–ligand assembly:

With appropriate installation of chiral chromophores, CD spectroscopy can provide useful structural information for complicated dynamic processes in solution that are difficult to probe otherwise. Our UV/Vis and fluorescence spectroscopic titration studies on L2^R (Figure 7) have revealed systematic spectral shifts and correlated changes in signal intensities upon metallation. These observations are consistent with the simple 1:1 binding model involving two chromogenic/fluorogenic species, that is, free and metallated ligands (Scheme 2). This interpretation was further supported by the Job plot analysis (Figure S5 in the Supporting Information) and ^1H NMR (both 1D and 2D) spectroscopic studies (Figures 5 and 6, and Figure S3 in the Supporting Informa-

tion), which collectively established the 1:1 stoichiometry between the metal and the ligand. This chemically intuitive assembly model, however, was challenged by the CD titration studies described below.

To study the evolution of helicity as a function of metal loading, we first monitored the CD intensity of L2^R at $\lambda = 330$ nm upon addition of zinc(II). As anticipated, the CD band displayed an increase in its intensity with increasing Zn^{2+} concentration. In contrast to our anticipated result, however, the signal intensity reached its maximum value at only 0.7 equivalents of metal with respect to the ligand (Figure 9a). After this point, a gradual decrease in the CD in-

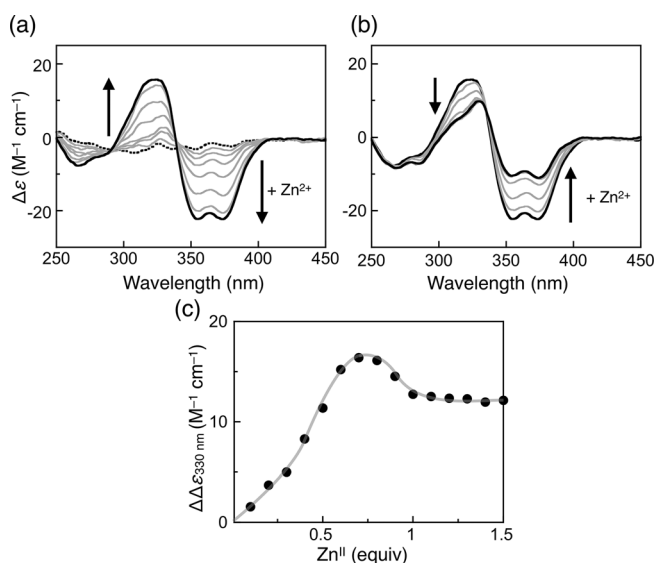


Figure 9. CD spectra of L2^R ($10 \mu\text{M}$ in MeCN; $T = 298$ K) measured after addition of $\text{Zn}(\text{OTf})_2$: a) 0–0.7 and b) 0.7–1.5 equivalents. c) A plot of $\Delta\epsilon_{330 \text{ nm}}$ (that is, the change in the intensity of the Cotton effect at $\lambda = 330$ nm) versus the amount of zinc(II) (in equiv).

tensity was observed (Figure 9b). Beyond one equivalent of Zn^{2+} , the signal remained invariant (Figure 9c), implying that the chemical equilibrium between the metal and ligand has been fully established.

A similar phenomenon was observed for another pineno-[4,5]-fused ligand L3^S (Figure S11 in the Supporting Information), suggesting that this rather peculiar behaviour is not an experimental artefact. This observation rather suggests the involvement of intermediate species in the conversion of the free ligand into the discrete 1:1 metal complex. It should be noted that such a stepwise process was not observable by titration using either UV/Vis (Figure 7a) or fluorescence (Figure 7b) spectroscopy, neither showing apparent accumulation of intermediates.

We thus re-visited the equilibrium in solution by using ^1H NMR spectroscopy to probe the nature of the CD-active species that are not the final assembly product $[\text{Zn}(\text{L2}^R)(\text{OTf})_2]$. As shown in Figure 10, a sample of L2^R in CDCl_3 treated intentionally with a substoichiometric amount (0.5 equiv) of $\text{Zn}(\text{OTf})_2$ revealed highly broadened and com-

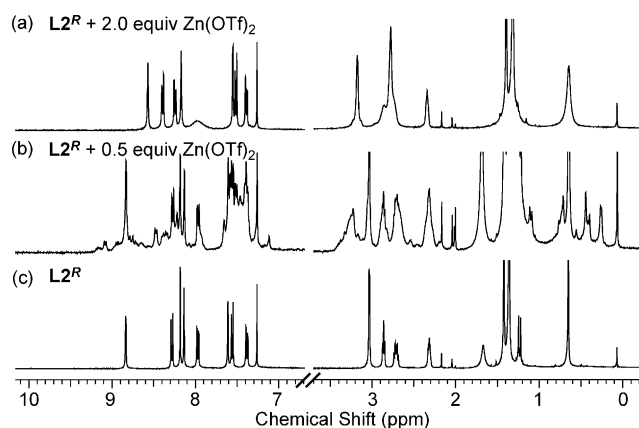


Figure 10. Partial ^1H NMR spectra of L2^R (10 mM in CDCl_3 ; $T=298$ K) obtained after addition of $\text{Zn}(\text{OTf})_2$: a) 2.0, b) 0.5 and c) 0 equivalents.

plicated spectral patterns (Figure 10b), which are different from those found for the free ligand L2^R (Figure 10c) or the isolated metal complex $[\text{Zn}(\text{L2}^R)(\text{OTf})_2]$ (Figure 5a). Further addition of $\text{Zn}(\text{OTf})_2$, however, significantly simplified the spectrum, which eventually became identical to that of $[\text{Zn}(\text{L2}^R)(\text{OTf})_2]$ (Figures 5a and 10a).

Such metal-ion-concentration-dependent changes in the ^1H NMR spectra and the eventual formation of the discrete 1:1 complex with increasing amount of metal ions imply the evolution and decay of multiple adducts of different metal-to-ligand stoichiometry. In support of this notion, MALDI and ESI mass spectrometric analysis of the reaction mixture prepared with 0.5 equivalents of zinc(II) (as described in Figure 10b), revealed the existence of the 1:2 and 1:3 adducts, that is, $[\text{Zn}(\text{L2}^R)_2]^{2+}$ and $[\text{Zn}(\text{L2}^R)_3]^{2+}$, in addition to the anticipated 1:1 adduct and the free ligand (Figure S12 in the Supporting Information).

Thermodynamically driven ligand exchange: The observation of slowly exchanging intermediates derived from zinc(II) and L2^R (Figure 10 and Figure S12 in the Supporting Information) prompted us to investigate their interconversion in solution. We postulated that exogenously added nitrogen donor ligands, such as pyridine, should accelerate ligand exchange (either in an associative or dissociative mechanism) between the initially formed adducts, and facilitate the entropically driven transformation of the various $[\text{Zn}(\text{L2}^R)_n]^{2+}$ ($n=2$ or 3) species (Scheme 3) into the 1:1 adduct $[\text{Zn}(\text{L2}^R)]^{2+}$. Indeed, addition of an excess (5000 equiv) of pyridine to a 2:1 mixture of L2^R and $\text{Zn}(\text{OTf})_2$ elicited an immediate decrease in the intensity of the ECCD couplet (Figure 11a). Under similar conditions, the CD spectrum of $[\text{Zn}(\text{L2}^R)(\text{OTf})_2]$ showed a negligible change (Figure 11c). These findings confirm that, once formed, the 1:1 complex retains its structural integrity against ligand exchange with pyridine.

For both samples that were treated with pyridine and studied by CD spectroscopy (Figure 11a, c), the corresponding UV/Vis spectra remained essentially invariant (Figure 11b, d). Therefore, the decrease in the CD signal inten-

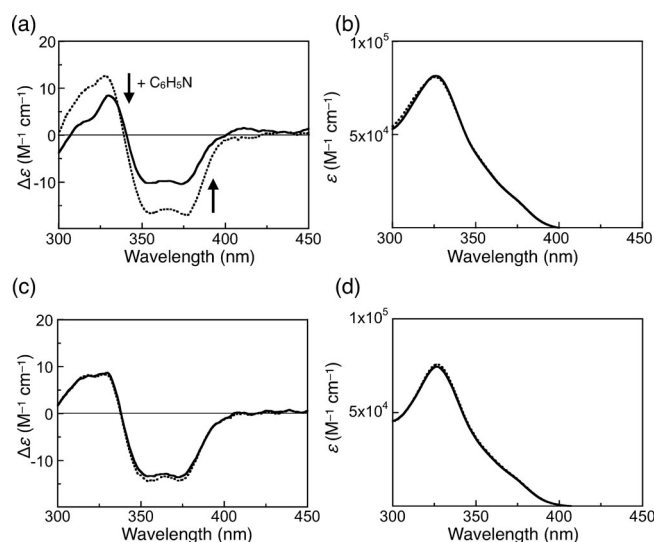


Figure 11. a) CD and b) UV/Vis spectra of a 2:1 mixture of L2^R (10 μM) and $\text{Zn}(\text{OTf})_2$ in MeCN prior to (dotted lines) and after (solid lines) addition of an excess (5000 equiv) of pyridine at $T=298$ K. Shown for comparison are the c) CD and d) UV/Vis spectra of $[\text{Zn}(\text{L2}^R)(\text{OTf})_2]$ obtained under similar reaction conditions.

sity shown in Figure 11a cannot be a consequence of loss of the bipy ligand from the metal centre. Rather, this behaviour reflects the exchange of one type of bipy ligand with another in the interconversion of various $[\text{Zn}(\text{L2}^R)_n]^{2+}$ species, which is indistinguishable by UV/Vis spectroscopy (Figure 11b) but readily discernible by CD spectroscopy (Figure 11a). Evidently, such ligand-exchange processes are repeated until the thermodynamically most stable 1:1 adduct dominates the population in solution.

Independent experimental evidence for this interpretation was provided by ^1H NMR spectroscopic studies, which are shown in Figure S13 in the Supporting Information. Upon treatment with $[\text{D}_5]$ pyridine (2500 equiv), the complicated ^1H NMR spectrum of $\text{L2}^R + \text{Zn}(\text{OTf})_2$ (0.5 equiv) transformed into to a simpler pattern comprised of two independent sets of proton resonances associated with the free ligand L2^R and 1:1 adduct $[\text{Zn}(\text{L2}^R)(\text{OTf})_2]$; no other species were spectroscopically detected. A coherent mechanistic model that is consistent with all our experimental observations is summarised in Scheme 3.

Metallation of “unlinked” chiral bipyridyl ligand models:

One important consideration behind the design of our chiral ligands (Figure 4) was the use of a rigid C_2 -symmetric arylene–ethynylene scaffold to link two chiral bipy units to restrict their conformational freedom (Schemes 1 and 2). Unlike self-assembly in solution from freely diffusing chiral components, restricted swivelling motions around the rigid aryl–aryl and/or aryl–ethynyl linkers should allow the bipy ligand to take a limited number of trajectories in space that converge to the metal centre to form a stable 1:1 adduct as the final adduct.

How would the system behave in the absence of such conformational restriction? More specifically, does the arylene–

ethynylene linker between the two chiral bipy units indeed play an important functional role, or is it structural “over-engineering” that does not offer any practical advantage over simpler bidentate systems in the chiral-selection process? To address this important scientific question, we carried out metallation studies on the simple chiral bipy derivative **6** (Scheme 5) as a bidentate “site model” for **L2^R**.

Although the CD spectrum of the free ligand **6** in MeCN is essentially featureless, a large negative couplet quickly emerged upon addition of Zn(OTf)₂ (Figure 12 a), which is similar to the behaviour of [Zn(**L2^R**)(OTf)₂] supported by the fully assembled tetra-dentate ligand (Figure 9 a).

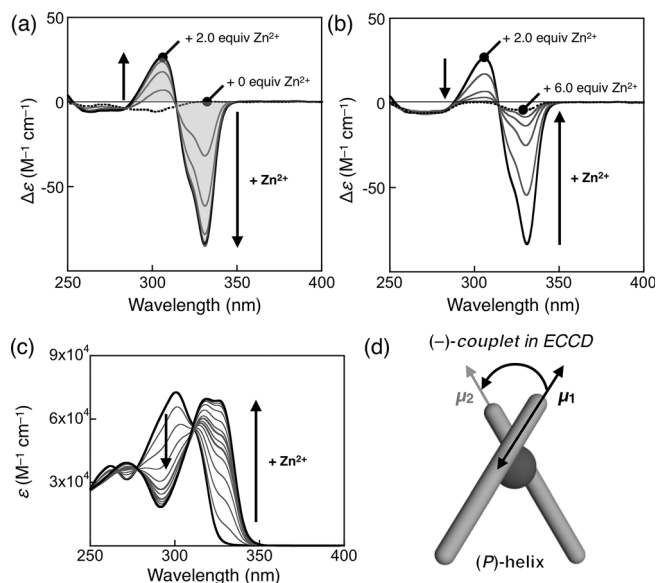


Figure 12. CD spectra of **6** (20 μM in MeCN; *T* = 298 K) measured after addition of Zn(OTf)₂: a) 0–2.0 and b) 2.0–6.0 equivalents. c) The UV/Vis spectra obtained under identical conditions, which show continuous spectral change across what appear to be isosbestic points. The negative ECCD couplet, shaded in (a), results from the through-space interaction between the two electric transition dipoles (designated as μ₁ and μ₂) of the (*P*)-helical stereoisomer as schematically shown in (d).

A change in the sign of the CD signal (ECCD) is the signature of inter-chromophore electronic coupling. For two interacting electric-transition dipoles that are configurationally or conformationally well-defined in terms of their relative orientations in space, the change in the sign of the Cotton effect, that is, a negative or positive couplet, allows for a direct assignment of the absolute screw-sense of helical twisting.^[17] Based on the ECCD model shown in Figure 12 d, the experimentally observed negative couplet corresponds to the (*P*)-helix.

Previous structural studies have established that pineno-[4,5]-fused bipy derivatives sharing the same absolute configuration as **2^R** (Scheme 4; synthetic precursor to **6**) typically support a right-handed Δ-isomer of (*P*)-helicity with a negative ECCD couplet.^[41–43] As anticipated, enantiomeric bipy ligands analogous to **2^S** (Scheme 4) afford Λ-helicates of (*M*)-helicity with a positive ECCD couplet,^[42,44] thereby

establishing a direct correlation between the ligand-based point chirality and the axial chirality created at the metal centre resulting from asymmetric inter-ligand steric bias. Consistent with this empirical trend, similar negative ECCD couplets are observed for both the tetra-dentate ligand **L2^R** (Figure 9) and the bi-dentate ligand **6** (Figure 12) upon metallation.^[45]

Unlike the behaviour of **L2^R** under similar conditions (Figure 9), however, the intensity of the ECCD signal from **6** + Zn(OTf)₂ continues to increase with up to approximately two equivalents of zinc(II) (Figure 12 a), but starts to decrease beyond this point. In the presence of a large excess (>6 equiv) of Zn(OTf)₂, only a very weak exciton couplet was observed (Figure 12 b). This metal-concentration-dependent spectral change suggests the initial formation of the bis(chelate) adduct [Zn(**6**)₂]²⁺ (Figure 13), and its subsequent disassembly into the 1:1 adduct [Zn(**6**)]²⁺ with increasing metal loading. Unlike [Zn(**6**)₂]²⁺, no intramolecular exciton coupling is allowed for [Zn(**6**)]²⁺, and therefore no strong ECCD signal was observed at high metal-to-ligand ratios.

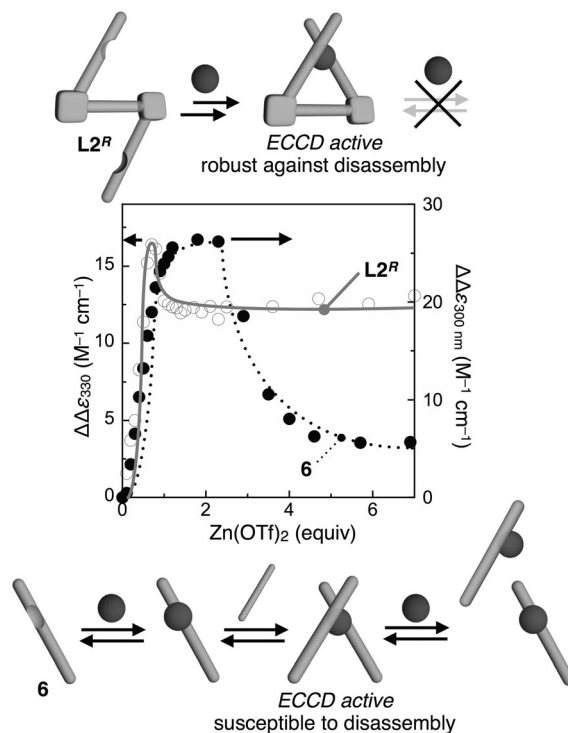


Figure 13. Models of structure assembly–disassembly of the metal complexes supported by bidentate **6** (bottom) and tetradentate **L2^R** (top) probed by metal-concentration-dependent changes in the CD signal intensities plotted as ΔΔε_{300 nm} (that is, the change in the intensity of the Cotton effect at λ = 300 nm) for **6** (●), and ΔΔε_{330 nm} (that is, the change in the intensity of the Cotton effect at λ = 330 nm) for **L2^R** (○) versus the amount of zinc(II) (in equiv) added.

Consistent with this equilibrium model in solution (Figure 13), the ¹H NMR spectrum of **6** treated with one equivalent Zn(OTf)₂ (Figure 14 b) revealed the development

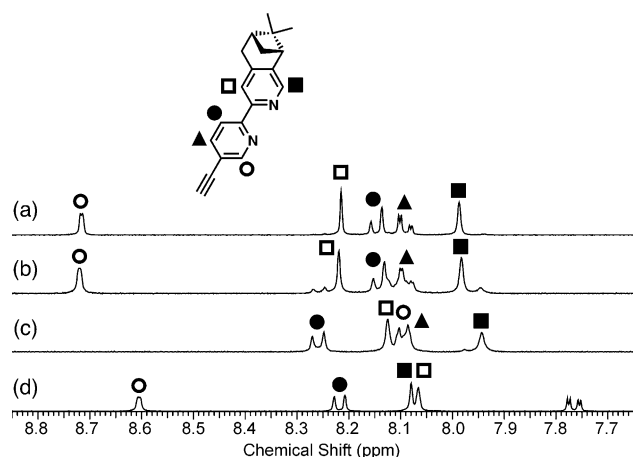


Figure 14. Partial ^1H NMR spectra of **6** (10 mM) in $\text{CDCl}_3/\text{CD}_3\text{CN}$ (4:1, v/v) obtained after addition of $\text{Zn}(\text{OTf})_2$ at $T=298\text{ K}$ (a) 2.0, b) 1.0 and c) 0.5 equivalents) compared with that of the free ligand **6** shown in (d).

of two independent sets of proton resonances, assigned to $[\text{Zn}(\mathbf{6})_2]^{2+}$ and $[\text{Zn}(\mathbf{6})]^{2+}$ (Figure 13). In support of this notion, HR-ESI mass spectrometric analysis confirmed the presence of both $[\text{Zn}(\mathbf{6})_2]^{2+}$ and $[\text{Zn}(\mathbf{6})]^{2+}$ species in the solution (Figures S14 and S15 in the Supporting Information). On the other hand, samples prepared with either lower (0.5 equiv of $\text{Zn}(\text{OTf})_2$; Figure 14c) or higher (2 equiv of $\text{Zn}(\text{OTf})_2$; Figure 14a) loadings of the metal ion furnished simple ^1H NMR spectral patterns dominated by the 1:2 and 1:1 complexes, $[\text{Zn}(\mathbf{6})_2]^{2+}$ and $[\text{Zn}(\mathbf{6})]^{2+}$, respectively.

Additional experimental support for our assembly–disassembly model shown in Figure 13 came from independent CD titration studies of **6** by using ZnCl_2 instead of $\text{Zn}(\text{OTf})_2$. We anticipated that the strongly coordinating chloride ligand would prevent formation of the bis(chelate) complexes such as $[\text{Zn}(\mathbf{6})_2]^{2+}$. Indeed, the CD spectra obtained for the reaction mixture **6** + ZnCl_2 in MeCN (Figure S16 in the Supporting Information) did not show the strong ECCD couplet observed for **6** + $\text{Zn}(\text{OTf})_2$ (Figure 12). Even with an increased amount of ZnCl_2 , only a weak CD signal was observed, which eventually became identical to that of **6** in the presence of a large excess of $\text{Zn}(\text{OTf})_2$.

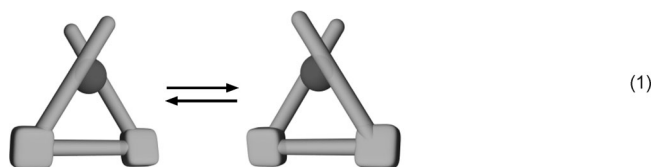
Although the CD spectroscopy provided significant insights into the complicated dynamics in solutions involving multiple metal-containing species, the corresponding UV/Vis spectra (Figure 12c and Figure S16 in the Supporting Information) show a correlated increase and decrease in the chromophore population across what could be considered to be isosbestic points. These UV/Vis data thus wrongly implicate simple interconversion between two equilibrating species, which is far from what is actually occurring in solution (Figure 13). Most importantly, the metal-concentration-dependent structural assembly and disassembly observed for the simple bidentate ligand system **6** (Figures 12 and 13) stands in stark contrast to the stability of $[\text{Zn}(\mathbf{L}2^R)(\text{OTf})_2]$ exposed to excess $\text{Zn}(\text{OTf})_2$ (Figures 9 and 13). Once formed, the mononuclear complex of the “linked bis(bipy)”

ligand maintains its structural integrity, as shown by the lack of changes in the ECCD intensity even after addition of a large excess of metal ions beyond the 1:1 stoichiometric point.

Collectively, Scheme 3 and Figure 13 describe the ligand-dependent and metal-dependent solution-state dynamics that we have established experimentally for the chiral tetra- and bi-dentate ligand systems, respectively. A detailed understanding of this actual assembly–disassembly process was obtained by ECCD spectroscopy, which directly and sensitively monitors changes in the spatial relationship between the chiral chromophores constituting the metal coordination sphere. Our comparative studies on the simple pinene-fused bipy system **6** and its “linked” derivative $\mathbf{L}2^R$ convincingly demonstrated that structural pre-organisation and chelate effects play a critical role in the thermodynamic stability of the metal complex.

Configurational stability: Selection and switching of metal-based chirality:

Once formed, mono-nuclear zinc(II) complexes supported by the bi-dentate ligand **6** or the tetra-dentate ligand $\mathbf{L}2^R$ both display negative ECCD couplets suggestive of (*P*)-helicity. We noted, however, that the absolute magnitude of the change in ellipticity ($\Delta\Delta\epsilon \approx 12\text{ M}^{-1}\text{ cm}^{-1}$ at $\lambda=330\text{ nm}$) of $[\text{Zn}(\mathbf{L}2^R)(\text{OTf})_2]$ is significantly lower than that ($\Delta\Delta\epsilon \approx 27\text{ M}^{-1}\text{ cm}^{-1}$ at $\lambda=300\text{ nm}$) of its bis(chelate) analogue $[\text{Zn}(\mathbf{6})_2]^{2+}$ (Figure 13). This observation raised the possibility that a fast interconversion between the (*P*)- and (*M*)-isomer [Eq. (1)] might occur at room temperature if the steric bias imposed by the pinene-fused bipy motifs is not sufficiently large to differentiate them energetically.



Unlike previously reported chiral bipy complexes of zinc(II),^[38,39] the ^1H NMR spectra of $[\text{Zn}(\mathbf{L}2^R)(\text{OTf})_2]$ (Figures 5 and 6) and $[\text{Zn}(\mathbf{L}3^S)(\text{OTf})_2]$ (Figure S17 in the Supporting Information) showed only one set of proton resonances at $T=298\text{ K}$. Upon lowering the temperature, however, the spectrum revealed the presence of the two diastereomers (Figure 15).

Fortuitously, these two species exchange sufficiently slowly to allow for the determination of the coalescence temperature (T_c) and the activation barrier of isomerisation [ΔG^\ddagger for Eq. (1)] at T_c by using Equations (2) and (3), in which k_c is the exchange rate; $\Delta\nu$ is the difference in resonance frequency; k is the Boltzmann constant; T_c is the coalescence temperature; h is the Planck constant; and R is the gas constant.

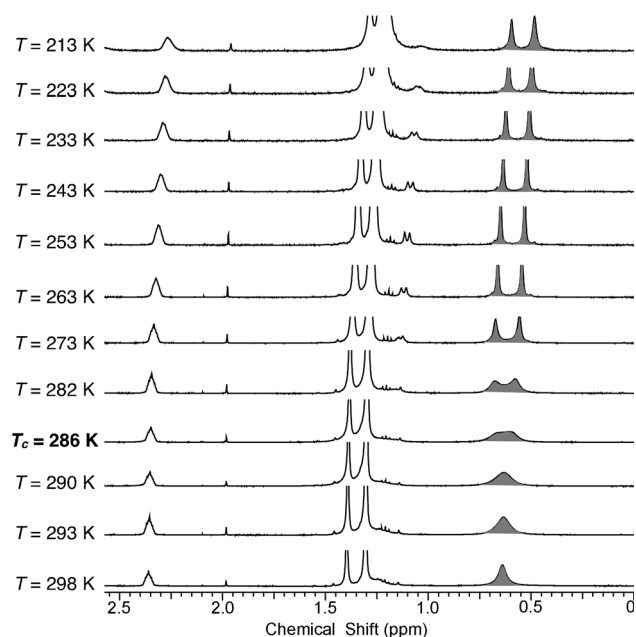


Figure 15. Temperature-dependent ($T=213$ – 298 K) changes in the ^1H NMR spectra (in CD_2Cl_2) of $[\text{Zn}(\text{L}2^{\text{R}})(\text{OTf})_2]$ in the aliphatic resonance region. The unresolved signals from the methyl groups belonging to each diastereomer [Eq. (1); shaded in grey] split at <286 K (shaded in red), which corresponds to the estimated exchange rate of $k_c=104$ s^{-1} at $T_c=279$ K.

$$k_c = \frac{\pi\Delta\nu}{\sqrt{2}} \quad (2)$$

$$k_c = \frac{kT_c}{h} e^{-\frac{\Delta G^\ddagger}{RT_c}} \quad (3)$$

The estimated ΔG^\ddagger values were 14.1 and 13.7 kcal mol^{-1} for $[\text{Zn}(\text{L}2^{\text{R}})(\text{OTf})_2]$ (at $T=286$ K) and $[\text{Zn}(\text{L}3^{\text{S}})(\text{OTf})_2]$ (at $T=279$ K), respectively, in CD_2Cl_2 . The similar activation parameters obtained for these two complexes suggest that the subtle difference in the stereochemistry of the [4,5]-fused pineno group does not significantly influence the energetics of chirality switching between the (*M*)- and (*P*)-isomers [Eq. (1)]. Comparative studies on the bis(chelate) complex, $[\text{Zn}(\mathbf{6})_2(\text{OTf})_2]$, generated in situ by treating $\mathbf{6}$ with 0.5 equivalents of $\text{Zn}(\text{OTf})_2$, provided a similar ΔG^\ddagger value of 12.7 kcal mol^{-1} (Figure S18 in the Supporting Information). Evidently, steric constraints imposed by the rigid and C_2 -symmetric arylene-ethynylene backbone do not significantly influence the inherent activation barrier for the helicity switching of the metal complexes supported by this particular chiral bipy ligand.

The relatively small ΔG^\ddagger values (12.7 – 14.1 kcal mol^{-1}) of stereochemical interconversion observed for $[\text{Zn}(\text{L}2^{\text{R}})(\text{OTf})_2]$, $[\text{Zn}(\text{L}3^{\text{S}})(\text{OTf})_2]$ and $[\text{Zn}(\mathbf{6})_2(\text{OTf})_2]$ suggest that the isomerisation process most likely proceeds through non-dissociative pathways, such as trigonal or rhombic twist mechanisms.^[46,47] Previous studies on $[\text{Cu}(\text{bipy}^*)_2]^+$ (bipy^* = chiral bipy ligand derivative) complexes of the kinetically labile d^{10} metal system determined similar activation param-

eters (10 – 16 kcal mol^{-1}) for the isomerisation between (*P*)- and (*M*)-isomers, proceeding through non-dissociative mechanisms.^[48]

Conclusion

With appropriate ligand design, metal complexes of kinetically labile d^{10} systems readily undergo dynamic assembly–disassembly processes in solution to expedite the evolution of a single dominant structure. Through repetitive self-correction processes involving facile formation and cleavage of metal–ligand bonds, energetically less stable earlier adducts quickly converge to the thermodynamically most stable final product, in a manner reminiscent of macromolecular folding through the disassembly and reassembly of multiple non-covalent bonds. Our studies on the zinc(II) complexes of chiral tetra-dentate ligands have revealed the “not-so-simple” stereodynamic processes of metal–ligand assembly and helicity switching, which are disguised by apparently “simple” spectral patterns.

We have shown that what appear to be straightforward spectroscopic features obtained by UV/Vis and fluorescence spectroscopy, which are often used as the primary diagnostic methods to study metal–ligand assembly, could provide an oversimplified and inaccurate picture of the actual equilibrium in solution. By using ECCD spectroscopy as the structure-sensitive spectroscopic tool, we have experimentally confirmed: 1) the reaction pathways of metal–ligand assembly involving multiple, slowly exchanging species; 2) the thermodynamic stability provided by the conformationally rigid and π -conjugated ligand skeleton; and 3) the kinetic lability responsible for the *P*-to-*M* (and vice versa) helicity switching and the mechanistic implications of the energy barrier. Although the preferred screw sense seems to still be dictated by the sterically less-congested conformation, the small energetic bias and low activation barrier in the chiral selection need to be improved in future ligand design based on these proof-of-concept prototypes. Efforts in such directions are currently under way in our laboratory.

Acknowledgements

This work was supported by the National Science Foundation (CHE 0547251) and the U.S. Army Research Office (W911NF-07-1-0533).

- [1] a) A. von Zelewsky, *Stereochemistry of Coordination Compounds*, Wiley, Chichester, **1996**; b) J.L. Pierre, *Coord. Chem. Rev.* **1998**, *178*, 1183–1192; c) H. Brunner, *Angew. Chem.* **1999**, *111*, 1248–1263; *Angew. Chem. Int. Ed.* **1999**, *38*, 1194–1208; d) U. Knof, A. von Zelewsky, *Angew. Chem.* **1999**, *111*, 312–333; *Angew. Chem. Int. Ed.* **1999**, *38*, 302–322; e) C. Ganter, *Chem. Soc. Rev.* **2003**, *32*, 130–138; f) P. D. Knight, P. Scott, *Coord. Chem. Rev.* **2003**, *242*, 125–143; g) J. Lacour, V. Hebbe-Viton, *Chem. Soc. Rev.* **2003**, *32*, 373–382; h) H. Amouri, M. Gruselle, *Chirality in Transition Metal Chemistry: Molecules, Supramolecular Assemblies and Materials*,

- Wiley, Chichester, **2009**; i) J. Crassous, *Chem. Commun.* **2012**, *48*, 9684–9692.
- [2] a) J. W. Steed, J. L. Atwood, *Supramolecular Chemistry*, 2nd ed., Wiley, Chichester, **2009**; b) J. R. Nitschke, *Acc. Chem. Res.* **2007**, *40*, 103–112; c) S. J. Lee, W. Lin, *Acc. Chem. Res.* **2008**, *41*, 521–537; d) J. Crassous, *Chem. Soc. Rev.* **2009**, *38*, 830–845.
- [3] For a thematic issue on Enantioselective Catalysis, see: *Chem. Rev.* **2003**, *103*, 8, 2761–3400.
- [4] a) T. P. Yoon, E. N. Jacobsen, *Science* **2003**, *299*, 1691–1693; b) *New Frontiers in Asymmetric Catalysis* (Eds.: K. Mikami, M. Lautens), Wiley, Hoboken, **2007**; c) M. Shibasaki, M. Kanai, S. Matsunaga, N. Kumagai, *Acc. Chem. Res.* **2009**, *42*, 1117–1127; d) E. B. Bauer, *Chem. Soc. Rev.* **2012**, *41*, 3153–3167.
- [5] a) E. A. Hillard, G. Jaouen, *Organometallics* **2011**, *30*, 20–27; b) E. Meggers, *Angew. Chem.* **2011**, *123*, 2490–2497; *Angew. Chem. Int. Ed.* **2011**, *50*, 2442–2448; c) E. Meggers, *Eur. J. Inorg. Chem.* **2011**, 2911–2926.
- [6] a) B. M. Zeglis, V. C. Pierre, J. K. Barton, *Chem. Commun.* **2007**, 4565–4579; b) M. J. Hannon, *Chem. Soc. Rev.* **2007**, *36*, 280–295; c) F. R. Keene, J. A. Smith, J. G. Collins, *Coord. Chem. Rev.* **2009**, *253*, 2021–2035; d) H. Yang, K. L. Metera, H. F. Sleiman, *Coord. Chem. Rev.* **2010**, *254*, 2403–2415; e) H.-K. Liu, P. J. Sadler, *Acc. Chem. Res.* **2011**, *44*, 349–359; f) M. R. Gill, J. A. Thomas, *Chem. Soc. Rev.* **2012**, *41*, 3179–3192.
- [7] For a recent review on chiral helicates, see: S. E. Howson, P. Scott, *Dalton Trans.* **2011**, *40*, 10268–10277.
- [8] a) Y. Chen, S. Yekta, A. K. Yudin, *Chem. Rev.* **2003**, *103*, 3155–3212; b) J. M. Brunel, *Chem. Rev.* **2005**, *105*, 857–898.
- [9] a) R. Noyori, H. Takaya, *Acc. Chem. Res.* **1990**, *23*, 345–350; b) R. Noyori, *Angew. Chem.* **2002**, *114*, 2108–2123; *Angew. Chem. Int. Ed.* **2002**, *41*, 2008–2022.
- [10] a) P. Kočovský, Š. Vyskočil, M. Smrčina, *Chem. Rev.* **2003**, *103*, 3213–3246; b) A. K. Unni, N. Takenaka, H. Yamamoto, V. H. Rawal, *J. Am. Chem. Soc.* **2005**, *127*, 1336–1337.
- [11] a) S. Schenker, A. Zamfir, M. Freund, S. B. Tsogoeva, *Eur. J. Org. Chem.* **2011**, 2209–2222; b) T. Akiyama, J. Itoh, K. Fuchibe, *Adv. Synth. Catal.* **2006**, *348*, 999–1010; c) T. Akiyama, *Chem. Rev.* **2007**, *107*, 5744–5758; d) A. Ting, S. E. Schaus, *Eur. J. Org. Chem.* **2007**, 5797–5815; e) S. J. Connon, *Angew. Chem.* **2006**, *118*, 4013–4016; *Angew. Chem. Int. Ed.* **2006**, *45*, 3909–3912; f) M. S. Taylor, E. N. Jacobsen, *Angew. Chem.* **2006**, *118*, 1550–1573; *Angew. Chem. Int. Ed.* **2006**, *45*, 1520–1543; g) A. G. Doyle, E. N. Jacobsen, *Chem. Rev.* **2007**, *107*, 5713–5743.
- [12] a) S. Sankararaman, G. Venkataramana, B. Varghese, *J. Org. Chem.* **2008**, *73*, 2404–2407; b) R. Nandy, M. Subramoni, B. Varghese, S. Sankararaman, *J. Org. Chem.* **2007**, *72*, 938–944.
- [13] S. Yagi, H. Kitayama, T. Takagishi, *J. Chem. Soc. Perkin Trans. 1* **2000**, 925–932.
- [14] a) D. Iwaniuk, C. Wolf, *J. Am. Chem. Soc.* **2011**, *133*, 2414–2417; b) D. P. Iwaniuk, C. Wolf, *Org. Lett.* **2011**, *13*, 2602–2605.
- [15] S. Toyota, *Chem. Rev.* **2010**, *110*, 5398–5424.
- [16] a) *Modern Acetylene Chemistry* (Eds.: P. J. Stang, F. Diederich), Wiley-VCH, Weinheim, **1995**; b) F. Diederich, P. J. Stang, R. R. Tykwinski in *Acetylene Chemistry: Chemistry, Biology and Material Science* (Eds.: F. Diederich, P. J. Stang, R. R. Tykwinski), Wiley-VCH, Weinheim, **2005**; c) V. Balzani, M. Venturi, A. Credi, *Molecular Devices and Machines: A Journey into the Nanoworld*, Wiley-VCH, Weinheim, **2003**; d) G. S. Kottas, L. I. Clarke, D. Horinek, J. Michl, *Chem. Rev.* **2005**, *105*, 1281–1376; e) T. F. Magnera, J. Michl, *Top. Curr. Chem.* **2005**, *262*, 63–97; f) T. C. Bedard, J. S. Moore, *J. Am. Chem. Soc.* **1995**, *117*, 10662–10671; g) J. S. Moore, *Acc. Chem. Res.* **1997**, *30*, 402–413; h) S. D. Karlen, M. A. Garcia-Garibay, *Top. Curr. Chem.* **2005**, *262*, 179–227; i) T.-A. V. Khuong, J. E. Nuñez, C. E. Godinez, M. A. Garcia-Garibay, *Acc. Chem. Res.* **2006**, *39*, 413–422; j) P. D. Jarowski, K. N. Houk, M. A. Garcia-Garibay, *J. Am. Chem. Soc.* **2007**, *129*, 3110–3117; k) Y. Shirai, J.-F. Morin, T. Sasaki, J. M. Guerrero, J. M. Tour, *Chem. Soc. Rev.* **2006**, *35*, 1043–1055; l) G. Vives, J. M. Tour, *Acc. Chem. Res.* **2009**, *42*, 473–487.
- [17] a) N. Berova, K. Nakanishi, in *Circular Dichroism: Principles and Applications*, 2nd ed. (Eds.: N. Berova, K. Nakanishi, R. W. Woody), Wiley-VCH, Weinheim, **2000**, pp. 337–382; b) N. Berova, L. D. Bari, G. Pescitelli, *Chem. Soc. Rev.* **2007**, *36*, 914–931; c) N. Berova, G. Pescitelli, A. G. Petrovic, G. Proni, *Chem. Commun.* **2009**, 5958–5980.
- [18] J. W. Canary, S. Mortezaei, J. Liang, *Chem. Commun.* **2010**, *46*, 5850–5860.
- [19] D. Leung, S. O. Kang, E. V. Anslyn, *Chem. Soc. Rev.* **2012**, *41*, 448–479.
- [20] a) T. Kurtán, N. Nesnas, Y.-Q. Li, X. Huang, K. Nakanishi, N. Berova, *J. Am. Chem. Soc.* **2001**, *123*, 5962–5973; b) T. Kurtán, N. Nesnas, F. E. Koehn, Y.-Q. Li, K. Nakanishi, N. Berova, *J. Am. Chem. Soc.* **2001**, *123*, 5974–5982; c) G. Proni, G. Pescitelli, X. Huang, N. Q. Quraishi, K. Nakanishi, N. Berova, *Chem. Commun.* **2002**, 1590–1591; d) X. Huang, N. Fujioka, G. Pescitelli, F. E. Koehn, R. T. Williamson, K. Nakanishi, N. Berova, *J. Am. Chem. Soc.* **2002**, *124*, 10320–10335; e) G. Proni, G. Pescitelli, X. Huang, K. Nakanishi, N. Berova, *J. Am. Chem. Soc.* **2003**, *125*, 12914–12927; f) M. Balaz, M. De Napoli, A. E. Holmes, A. Mamma, K. Nakanishi, N. Berova, R. Purrello, *Angew. Chem.* **2005**, *117*, 4074–4077; *Angew. Chem. Int. Ed.* **2005**, *44*, 4006–4009.
- [21] a) S. Zahn, J. W. Canary, *Org. Lett.* **1999**, *1*, 861–864; b) A. E. Holmes, D. Das, J. W. Canary, *J. Am. Chem. Soc.* **2007**, *129*, 1506–1507.
- [22] a) L. A. Joyce, M. S. Maynor, J. M. Dragna, G. M. da Cruz, V. M. Lynch, J. W. Canary, E. V. Anslyn, *J. Am. Chem. Soc.* **2011**, *133*, 13746–13752; b) L. You, J. S. Berman, E. V. Anslyn, *Nat. Chem.* **2011**, *3*, 943–948; c) L. You, G. Pescitelli, E. V. Anslyn, L. Di Bari, *J. Am. Chem. Soc.* **2012**, *134*, 7117–7125; d) L. You, J. S. Berman, A. Lucksanawichien, E. V. Anslyn, *J. Am. Chem. Soc.* **2012**, *134*, 7126–7134; e) J. M. Dragna, G. Pescitelli, L. Tran, V. M. Lynch, E. V. Anslyn, L. Di Bari, *J. Am. Chem. Soc.* **2012**, *134*, 4398–4407.
- [23] a) S. Nieto, V. M. Lynch, E. V. Anslyn, H. Kim, J. Chin, *Org. Lett.* **2008**, *10*, 5167–5170; b) S. Nieto, V. M. Lynch, E. V. Anslyn, H. Kim, J. Chin, *J. Am. Chem. Soc.* **2008**, *130*, 9232–9233.
- [24] a) V. V. Borovkov, J. M. Lintuluoto, Y. Inoue, *Org. Lett.* **2000**, *2*, 1565–1568; b) V. V. Borovkov, J. M. Lintuluoto, Y. Inoue, *J. Am. Chem. Soc.* **2001**, *123*, 2979–2989; c) Q. Yang, C. Olmsted, B. Borhan, *Org. Lett.* **2002**, *4*, 3423–3426.
- [25] X. Jiang, B. G. Park, J. A. Riddle, B. J. Zhang, M. Pink, D. Lee, *Chem. Commun.* **2008**, 6028–6030.
- [26] For a related tetra-dentate ligand built with bis(picolate) donor groups, a tetrazinc(II) complex was isolated, see: B. G. Park, M. Pink, D. Lee, *J. Organomet. Chem.* **2011**, *696*, 4039–4045.
- [27] a) P. Hayoz, A. von Zelewsky, *Tetrahedron Lett.* **1992**, *33*, 5165–5168; b) P. Hayoz, A. von Zelewsky, H. Stoeckli-Evans, *J. Am. Chem. Soc.* **1993**, *115*, 5111–5114.
- [28] a) E. C. Constable, P. J. Steel, *Coord. Chem. Rev.* **1989**, *93*, 205–223; b) C. Kaes, A. Katz, M. W. Hosseini, *Chem. Rev.* **2000**, *100*, 3553–3590.
- [29] a) A. von Zelewsky, *Coord. Chem. Rev.* **1999**, *190–192*, 811–825; b) A. von Zelewsky, O. Mamula, *J. Chem. Soc. Dalton Trans.* **2000**, 219–231.
- [30] N. C. Fletcher, *J. Chem. Soc. Perkin Trans. 1* **2002**, 1831–1842.
- [31] G. Chelucci, R. P. Thummel, *Chem. Rev.* **2002**, *102*, 3129–3170.
- [32] M. Düggele, C. Goujon-Ginglinger, S. R. Ducotterd, D. Mauron, C. Bonte, A. v. Zelewsky, H. Stoeckli-Evans, A. Neels, *Org. Biomol. Chem.* **2003**, *1*, 1894–1899.
- [33] R. K. de Richter, M. Bonato, M. Follet, J. M. Kamenka, *J. Org. Chem.* **1990**, *55*, 2855–2860.
- [34] A. V. Malkov, I. R. Baxendale, M. Bella, V. Langer, J. Fawcett, D. R. Russell, D. J. Mansfield, M. Valko, P. Kočovský, *Organometallics* **2001**, *20*, 673–690.
- [35] H. C. Brown, S. A. Weissman, P. T. Perumal, U. P. Dhokte, *J. Org. Chem.* **1990**, *55*, 1217–1223.
- [36] K. D. Oyler, F. J. Coughlin, S. Bernhard, *J. Am. Chem. Soc.* **2007**, *129*, 210–217.

- [37] a) E. D. Mihelich, D. J. Eickhoff, *J. Org. Chem.* **1983**, *48*, 4135–4137; b) A. V. Malkov, D. Pernazza, M. Bell, M. Bella, A. Massa, F. Teplý, P. Meghani, P. Kočovský, *J. Org. Chem.* **2003**, *68*, 4727–4742; c) M. Mazzega, F. Fabris, S. Cossu, O. De Lucchi, V. Lucchini, G. Valle, *Tetrahedron* **1999**, *55*, 4427–4440.
- [38] C. Schaffner-Hamann, A. von Zelewsky, A. Barbieri, F. Barigelletti, G. Muller, J. P. Riehl, A. Neels, *J. Am. Chem. Soc.* **2004**, *126*, 9339–9348.
- [39] D. Lötscher, S. Rupprecht, P. Collomb, P. Belser, H. Viebrock, A. von Zelewsky, P. Burger, *Inorg. Chem.* **2001**, *40*, 5675–5681.
- [40] G. Baum, E. C. Constable, D. Fenske, C. E. Housecroft, T. Kulke, *Chem. Eur. J.* **1999**, *5*, 1862–1873.
- [41] H. Mürner, A. von Zelewsky, H. Stoeckli-Evans, *Inorg. Chem.* **1996**, *35*, 3931–3935.
- [42] D. Drahonovský, U. Knof, L. Jungo, T. Belser, A. Neels, G. C. Labat, H. Stoeckli-Evans, A. von Zelewsky, *Dalton Trans.* **2006**, 1444–1454.
- [43] For systems in which the pyridyl portion of the CHIRAGEN units are linked tightly through phenylene or ferrocenyl spacers, however, the stereochemical correlation is not straightforward, see: a) B. Quinodoz, G. Labat, H. Stoeckli-Evans, A. von Zelewsky, *Inorg. Chem.* **2004**, *43*, 7994–8004; b) K.-C. Sham, H.-L. Yeung, S.-M. Yiu, T.-C. Lau, H.-L. Kwong, *Dalton Trans.* **2010**, *39*, 9469–9471.
- [44] C. Hamann, A. von Zelewsky, A. Neels, H. Stoeckli-Evans, *Dalton Trans.* **2004**, 402–406.
- [45] The CD spectrum of $[\text{Zn}(\text{L}2^R)(\text{OTf})_2]$ (Figure 8) in the longer-wavelength end should have additional contributions from the twisted bis(ethynylphenyl) backbone where the HOMO and LUMO reside.^[25] The ECCD spectrum of the simpler model system $[\text{Zn}(\mathbf{6})_2(\text{OTf})_2]$ (Figure 12), however, does not suffer from such complications, allowing for an unambiguous assignment of the absolute helical sense based on the sharply defined bisignate features.
- [46] A. Rodger, B. F. G. Johnson, *Inorg. Chem.* **1988**, *27*, 3061–3062.
- [47] H. S. Rzepa, M. E. Cass, *Inorg. Chem.* **2007**, *46*, 8024–8031, and references therein.
- [48] a) V. Hebbe-Viton, V. Desvergnés, J. J. Jodry, C. Dietrich-Buchecker, J.-P. Sauvage, J. Lacour, *Dalton Trans.* **2006**, 2058–2065; b) V. Desvergnés-Breuil, V. Hebbe, C. Dietrich-Buchecker, J.-P. Sauvage, J. Lacour, *Inorg. Chem.* **2003**, *42*, 255–257; c) E. Riesgo, Y.-Z. Hu, F. Bouvier, R. P. Thummel, *Inorg. Chem.* **2001**, *40*, 2541–2546.

Received: November 26, 2012
Published online: February 28, 2013